ACS APPLIED MATERIALS & INTERFACES

Research Article

www.acsami.org

High Sensitivity and High Detection Specificity of Gold-Nanoparticle-Grafted Nanostructured Silicon Mass Spectrometry for Glucose Analysis

Chia-Wen Tsao* and Zhi-Jie Yang

Department of Mechanical Engineering, National Central University, Taoyuan City 32001, Taiwan

Supporting Information

ABSTRACT: Desorption/ionization on silicon (DIOS) is a high-performance matrix-free mass spectrometry (MS) analysis method that involves using silicon nanostructures as a matrix for MS desorption/ionization. In this study, gold nanoparticles grafted onto a nanostructured silicon (AuNPs-nSi) surface were demonstrated as a DIOS-MS analysis approach with high sensitivity and high detection specificity for glucose detection. A glucose sample deposited on the AuNPs-nSi surface was directly catalyzed to negatively charged gluconic acid molecules on a single AuNPs-nSi chip for MS analysis. The AuNPs-nSi surface was fabricated using two electroless deposition steps and one electroless etching step. The effects of the electroless fabrication parameters on the glucose detection efficiency were evaluated. Practical application of AuNPs-nSi MS glucose analysis in urine samples was also demonstrated in this study.

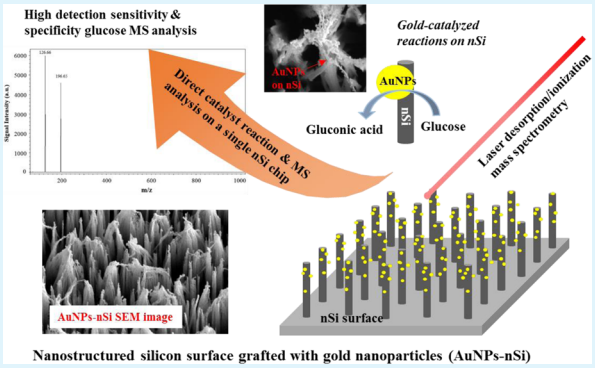

Nanostructured silicon surface grafted with gold nanoparticles (AuNPs-nSi)

KEYWORDS: *mass spectrometry, matrix-free laser desorption/ionization, desorption/ionization on silicon, nanostructured silicon, glucose analysis*

INTRODUCTION

Mass spectrometry (MS) is one of the most versatile analytical techniques and has been widely used in various fields, such as physics, chemistry, geology, materials science, environmental science, and so forth. Since the late 1980s, with the development of electrospray ionization mass spectrometry (ESI-MS)[1] and matrix-assisted laser desorption/ionization mass spectrometry (MALDI-MS),[2,3] MS has become a crucial tool for biological research. ESI-MS and MALDI-MS are well-established methods for analyzing macromolecules such as peptides, proteins, and oligonucleotides. However, these MS techniques have several limitations in small-molecule analysis. Biomolecules in MALDI-MS are ionized through a UV-absorbing organic matrix, and the organic matrix background in the low-mass range creates MS signal interference. In ESI-MS, biomolecules are ionized through electrostatic attraction, which generates multiple ion charges during MS analysis. The detection sensitivity of ESI-MS is typically lower than that of MALDI-MS

A desorption/ionization on silicon (DIOS) technique for analyzing small biomolecules using porous silicon[4,5] was reported in the 2000s. Various DIOS-related nanostructure surfaces, such as silicon nanowires,[6] nanofilament silicon,[7] nanostructured silicon (nSi),[8,9] silicon nanocones,[10] porous alumina,[11] and silicon nanowells,[12] have been demonstrated as effective nanostructure-based laser desorption/ionization mass spectrometry (LDI-MS) methods for analyzing small peptides or proteins. These techniques involve the use of nanoscale silicon structures as an organic matrix, absorbing laser energy to ionize biomolecules deposited onto a surface, thereby eliminating organic matrix background noise during LDI-MS analysis. The detection sensitivity of these DIOS-MS methods is typically high, and femtomole detection levels can be achieved. With a perfluorophenyl silylated porous silicon surface, detection sensitivity of des-Arg^9-bradykinin as high as 800 ymol was reported.[13] Because of these matrix-free and high detection sensitivity advantages, DIOS-MS is an ideal tool for analyzing small molecules and for applications in various other fields, including forensic polymer analysis,[14] drug abuse screening,[15,16] peptide sequencing,[17] and MS imaging.[18−21]

Glucose levels in blood or urine are widely recognized as a critical clinical indicator of diabetes mellitus.[22,23] Various glucose detection methods, such as optical,[24,25] photo-acoustic,[26] colorimetric,[27,28] surface plasmon resonance,[29] and electrochemical[30−35] approaches, have been demonstrated. These glucose detection methods are well-established and have been summarized in recent review articles.[31,33−37] Most of these techniques provide portability and low-cost advantages in

Received: August 11, 2015
Accepted: September 22, 2015
Published: September 22, 2015

DOI: 10.1021/acsami.5b07395
ACS Appl. Mater. Interfaces 2015, 7, 22630−22637

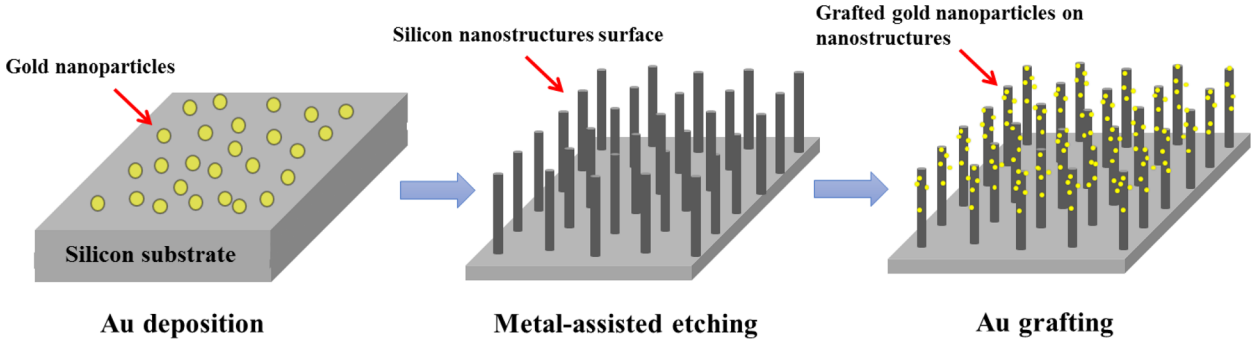

Figure 1. Schematic illustration of the fabrication of the Au-nanoparticle-grafted nanostructured silicon (AuNPs-nSi) surface.

glucose sensing. However, they may have problems with sensitivity or noise interference. For nonenzymatic electrochemical glucose sensors, the typical linear detection range is usually in the mM or μM range.[33−35] In addition to determining the glucose levels for diabetes mellitus, emerging research has shown that glucose is a potential biomarker for monitoring cancer development.[38,39] Therefore, creating an accurate, low sample consumption, and high-sensitivity glucose-level measurement tool is crucial for clinical diagnosis applications. Alternative to these glucose-sensing techniques, MS is a high sensitivity analytical tool that has been applied in glucose analysis. This is normally performed using the ESI-MS[40−42] approach. MALDI-MS for analyzing glucose samples has been less frequently reported because of background noise and ion suppression problems. Recently, 1-naphthylhydrazine hydrocholoride[43,44] and carbon nanodots[45] have been reported as a new matrix for MALDI-MS glucose analysis and have proven effective in real biological samples.

Nanostructure-based surfaces have been found to have little sensitivity to glucose samples during MS analysis. In this study, we used an nSi surface as a matrix-free DIOS-MS substrate for glucose analysis. An nSi surface grafted with Au nanoparticles was first demonstrated to directly catalyze the glucose sample into negatively charged gluconic acid ions for DIOS-MS analysis with high sensitivity and detection specificity on a single nSi surface. Fabrication of a Au-nanoparticle-grafted nanostructured silicon (AuNPs-nSi) surface and its effects on glucose MS analysis were evaluated. In addition, glucose was detected in a urine sample to demonstrate the effectiveness of the AuNPs-nSi MS approach in practical applications.

EXPERIMENTAL SECTION

Materials and Reagent Preparation. A P-type (100) single side polish silicon wafer 10 cm in diameter with a resistivity of 1−100 Ω cm was purchased from Summit-Tech Resource Corporation. Ethanol (EtOH, electronic grade), water (MS grade), acetone (HPLC grade), isopropyl alcohol (HPLC grade), and methanol (MeOH, 99.9%, electronic grade) were purchased from J.T. Baker. Hydrofluoric acid (HF, electronic grade, 49%) and hydrogen peroxide (H_2O_2, electronic grade, 31%) were purchased from BASF Corporation. D-Glucose powder (D-(+)-Glucose BioUltra, anhydrous, ≥99.5%) was purchased from Sigma-Aldrich. Hydrogen tetrachloroaurate(III) trihydrate ($HAuCl_4$, 99.99%) was purchased from Alfa Aesar.

A standard glucose sample was prepared by mixing the D-glucose powder with the MS-grade water at a series of concentrations ranging from 10^{-1} to 10^{-8} M. A urine sample was prepared by mixing the 10^{-3} M standard glucose sample with a participant's urine at a 1:1 volume ratio to achieve a 5×10^{-4} M concentration. The urine sample was then centrifuged at 5000 rpm for 2 min, and the supernatant was obtained for AuNPs-nSi MS analysis.

AuNPs-nSi Chip Fabrication. The AuNPs-nSi surface was fabricated using two electroless Au deposition (Au deposition and Au grafting) steps and one electroless etching (metal-assisted etching) step. A schematic illustration of the AuNPs-nSi fabrication process is shown in Figure 1.

The silicon substrate was first cleaned with acetone, isopropyl alcohol, DI water, and an ultrasonic sonicator bath for 3 min and then N_2 blow-dried to remove surface contaminates. Subsequently, the silicon substrate was immersed in a $HF/HAuCl_4$ (0.01 M/2.4 M) solution to deposit Au particles on the silicon surface. The Au-deposited silicon substrate was then rinsed with methanol and N_2 blow-dried to remove any excess $HF/HAuCl_4$ solution from the silicon surface. After Au deposition, the silicon substrate was immersed in HF/H_2O_2/EtOH (1:1:1 v/v/v) to create silicon nanostructures for 300 s. After etching, the substrate was fully rinsed with methanol and DI water and N_2 blow-dried to remove excess etchant from the surface.

After nSi surface fabrication, the Au grafting step was performed to graft the Au nanoparticles to the nSi surface. The nSi surface was placed in an O_2 plasma cleaner (PDC-32G, Harrick plasma) and treated (7.5×10^{-1} Torr, 18 W) for 60 s to change the nSi surface wettability. The O_2 plasma-treated nSi surface was immersed in the $HF/HAuCl_4$ (0.01 M/2.4 M) to graft Au nanoparticles. Finally, it was fully rinsed with methanol and DI water and N_2 blow-dried to create a AuNPs-nSi chip.

Mass Spectrometry Analysis. MS analysis of the AuNPs-nSi chip was performed using a standard MALDI-TOF mass spectrometer (Bruker autoflex speed MALDI TOF/TOF). In AuNPs-nSi MS analysis, a 5 μL sample was deposited on the AuNPs-nSi surface using a pipet and maintained for 900 s. Subsequently, the sample was N_2 blow-dried to remove the sample droplet from the AuNPs-nSi surface. The sample deposited on the AuNPs-nSi surface was then mounted onto a custom-machined nSi chip holder and transferred to a mass spectrometer for MS analysis. AuNPs-nSi MS analysis was conducted in linear and positive/negative-ion modes under a vacuum condition of $<3 \times 10^{-6}$ Torr. Optimized laser energy was set to 35% for the positive-ion mode and to 75% for the negative-ion mode. Each MS spectrum in this study was averaged from 150 laser pulses. The MS was calibrated on a MALDI-MS plate before MS analysis. Because AuNPs-nSi MS analysis and MALDI-MS calibration were not conducted on the same run, the AuNPs-nSi MS spectrum may be miscalibrated up to 1 Da.

Contact Angle Measurement. The water contact angle of silicon nanostructure surfaces was measured using a custom-made optical goniometer equipped with a high-resolution digital camera (Canon EOS 450D/TAMRON Macro 90 mm F2.8 lens), a z-axis precision stage, and a light source. A 5 μL water droplet was first pipetted on the AuNPs-nSi surface, and a side-view image of the microdroplet was then taken using the digital camera. The water contact angle was obtained by measuring the microdroplet tangent line and the solid surface from microdroplet images by using AutoCAD (Autodesk, Inc.) software.

DOI: 10.1021/acsami.5b07395
ACS Appl. Mater. Interfaces 2015, 7, 22630−22637

RESULTS AND DISCUSSION

Au Deposition and Metal-Assisted Etching for Nanostructured Silicon Fabrication. The Au nanoparticles were deposited on the silicon through a galvanic displacement reaction. Figure 2 shows the Au nanoparticle electroless deposition results for deposition times of 30, 60, 90, and 150 s. At 30 s (Figure 2a), round-shape nanoparticles 20−50 nm in diameter were uniformly deposited on the silicon surface. As the deposition time increased, the Au nanoparticles aggregated into oval- or island-shaped patterns, increasing in size to approximately 110 × 33 nm after 60 s (Figure 2b) and 240 × 40 nm after 90 s (Figure 2c). After 150 s of deposition (Figure 2d), the Au island-shaped nanoparticles further aggregated into a continuous Au thin film 350 × 50 nm in size on the surface.

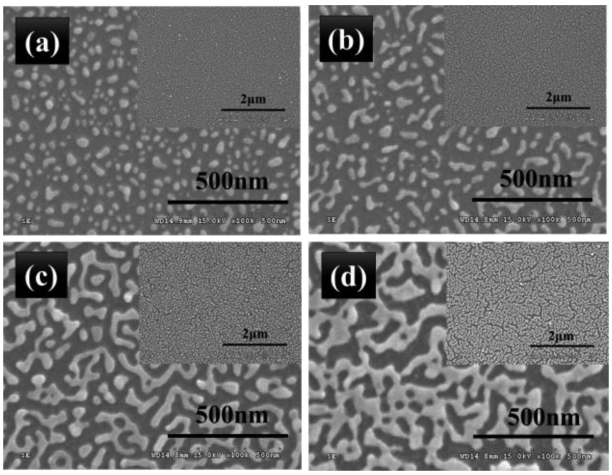

Figure 2. FESEM photograph of Au nanoparticles deposited on the silicon surface after immersion in the $HF/HAuCl_4$ solution for (a) 30, (b) 60, (c) 90, and (d) 150 s with 100× and 25× (top-right corner) magnification.

The nSi was then created a using a metal-assisted etching process.[46] In metal-assisted etching, the Au nanoparticles on the silicon substrate coated in the Au deposition step served as a cathode, and the silicon substrate served as an anode. Local electroless etching occurred at the Au/silicon interface, and each Au nanoparticle on the silicon surface was treated as a local etching site. The silicon underneath the Au nanoparticles was dissolved by a local electrochemical reaction to create silicon nanostructures, leaving the Au nanoparticles on the bottom of the nSi surface.[47] In a previous study, we demonstrated the electroless deposition step for creating an nSi surface. In this study, to maximize the amount of Au nanoparticles grafted to the nSi surface in the Au grafting procedure, we fabricated a silicon nanostructure morphology with a high surface/area ratio after metal-assisted etching. According to the nanoparticle deposition FESEM images shown in Figure 2, Au deposition for 30 s (Figure 2a) provided the densest Au nanoparticle distribution with the smallest nanoparticle size, which yields the largest surface/area silicon nanostructures. The nSi surface exhibit wire-shaped morphologies uniformly created on the silicon substrate with pores 200−350 nm in diameter and a height of 2.5 μm after etching (Figure S1).

Au Grafting for AuNPs-nSi. After nSi fabrication, Au grafting was performed to graft the Au nanoparticles onto the nanostructured surface to create a AuNPs-nSi surface. After metal-assisted etching, the silicon nanostructure exhibited high hydrophobicity with a water contact angle of approximately 145°. This high hydrophobicity surface nature limited the penetration of aqueous $HF/HAuCl_4$ into the silicon nanostructures, yielding optimal Au nanoparticle grafting performance. To solve this problem, we used O_2 plasma treatment to change the hydrophobic nSi into hydrophilic nSi. The water contact angle on the O_2-plasma-treated nSi surface measured approximately 5°. This showed that the hydrophobicity was extremely low, enabling improved penetration of the aqueous $HF/HAuCl_4$ solution into the silicon nanostructures, thus yielding optimal Au grafting performance. Three Au electroless grafting durations of 5, 10, and 15 s in the $HF/HAuCl_4$ mixture were used to evaluate Au grafting. Figure 3 shows a FESEM image of the top and cross-sectional views of the AuNPs-nSi surface after 5 s (Figure 3a,b), 10 s (Figure 3c,d), and 15 s (Figure 3e,f) Au grafting processes.

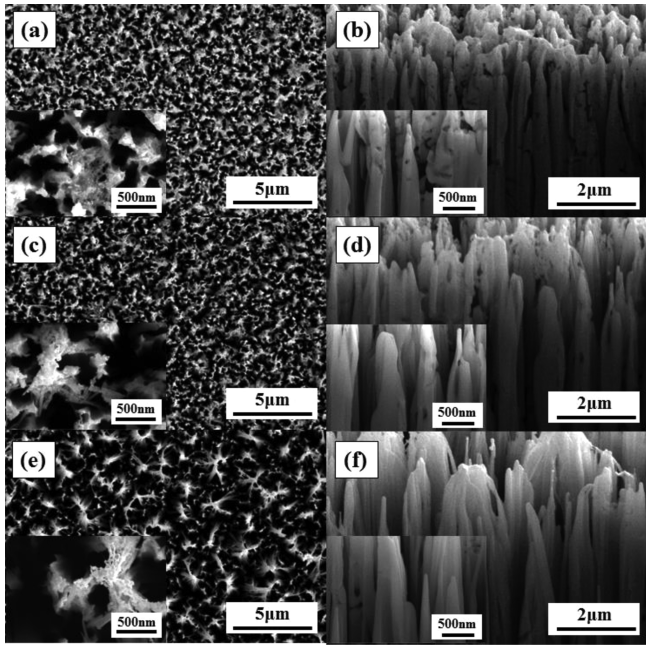

Figure 3. FESEM image of top (a, c, e) and 15° angle cross-sectional (b, d, f) view after 5, 10, and 15 s Au grafting processes.

After the Au grafting process, the nSi pore size increased. During the 5 s Au grafting process (Figure 3a), the pore size measured approximately 250−500 nm. After the Au grafting time was increased to 10 and 15 s, the silicon nanostructure pore size increased to 300−600 nm (Figure 3c) and 700−1200 nm (Figure 3e), respectively. The cross-sectional images in Figure 3b, d, and f show that the nanostructure morphology had no substantial variation after the grafting process. Numerous 20−50 nm pinholes were found at the wirelike silicon nanostructure sidewalls after grafting for all durations. These pinholes resulted from lateral HF etching, which facilitated the grafting of Au nanoparticles into the silicon nanostructure sidewalls during the electroless grafting procedure.

Figure 4 shows a 52° angle view of AuNPs-nSi surfaces subjected to electroless grafting for 5, 10, and 15 s. In the 52° angle and top images shown in Figure 4, white spots were observed at the tops of the nSi, as well as on the lateral surfaces, indicating the presence of Au nanoparticles grafted to the

DOI: 10.1021/acsami.5b07395
ACS Appl. Mater. Interfaces 2015, 7, 22630−22637

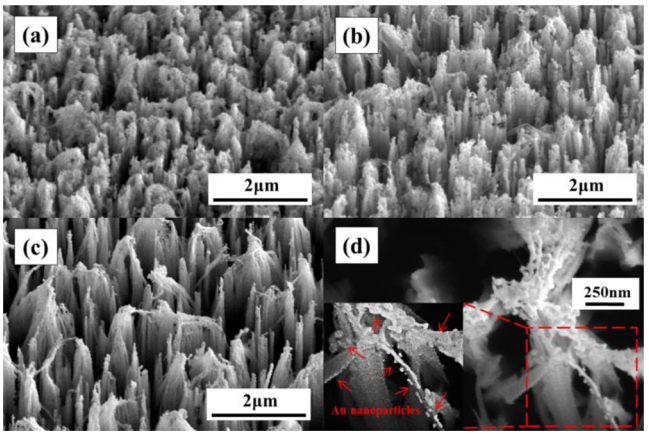

Figure 4. FESEM image providing a 52° angle view of the silicon surface after (a) 5 s, (b) 10 s, and (c) 15 s Au grafting processes. (d) Magnification (80×) of AuNPs-nSi chip subjected to electroless deposition for 30 s and electroless grafting for 15 s, showing Au nanoparticles grafted to the nanostructured silicon surface.

silicon nanostructures. In the 80× magnification FESME image shown in Figure 4d, the Au nanoparticles can be observed to be clearly grafted to the nSi surface.

EDS elemental analysis was performed in this study to evaluate the Au nanoparticle grafting performance. Figure 5 shows the EDS elemental mapping analysis results of the AuNPs-nSi chip top surface 5 s (Figure 5a), 10 s (Figure 5b), and 15 s (Figure 5c) after Au grafting. Original SEM images for EDS elemental analysis are shown on the left of Figure 5. EDS elemental analysis showed the presence of Si and Au on the AuNPs-nSi surface, as shown by the green mapping images in the middle and the red mapping images on the right of Figure 5, respectively. The EDS mapping results showed that the Au was uniformly distributed on the AuNPs-nSi surface. When the electroless grafting time was increased, more Au nanoparticles were found on the AuNPs-nSi surface.

Table 1 summarizes the quantified EDS elemental analysis results for AuNPs-nSi surfaces. The AuNPs-nSi surface grafted for 15 s exhibited the most Au with a 1.71% element weight percentage. Under the 10 s grafting condition, the weight percentage of Au decreased to 1.21%. We did not obtain the 5 s grafting result because the EDS elemental analysis instrument could not measure an element weight percentage less than 1%. However, the mapping image in Figure 6 shows that the Au nanoparticles were grafted to the nSi under the 5 s condition. The percentage of Au under the 5 s condition was estimated to be approximately 0.71%, assuming that the amount of Au nanoparticles grafted onto the nSi surface increased linearly with the grafting time.

Table 1. EDS Elemental Analysis of AuNPs-nSi Surfaces

test conditions	element	weight %
5 s	Si	99.29% [a]
2nd Au grafting	Au	0.71% [a]
10 s	Si	98.79%
2nd Au grafting	Au	1.21%
15 s	Si	98.29%
2nd Au grafting	Au	1.71%

[a]Estimated value.

AuNPs-nSi MS for Glucose Analysis. nSi-MS analysis provides several unique advantages; specifically, it requires no matrix and exhibits a high detection sensitivity. Although nSi-MS is ideal for small molecule analysis with high sensitivity, several types of small molecules, such as glucose, cannot be effectively ionized by the native nSi surface. Figure 6a shows a native nSi-MS spectrum in the positive-ion mode to analyze 10^{-1} M glucose. In the MS spectra shown in Figure 6a, numerous MS peaks can be observed below the 500 m/z range, and no glucose molecule signals appear at 181 m/z. Sodium adduct ion at 203 m/z can be observed among the MS peaks below 500 m/z. Other MS peaks are presumably noise peaks that may be attributable to sample or nSi surface contamination

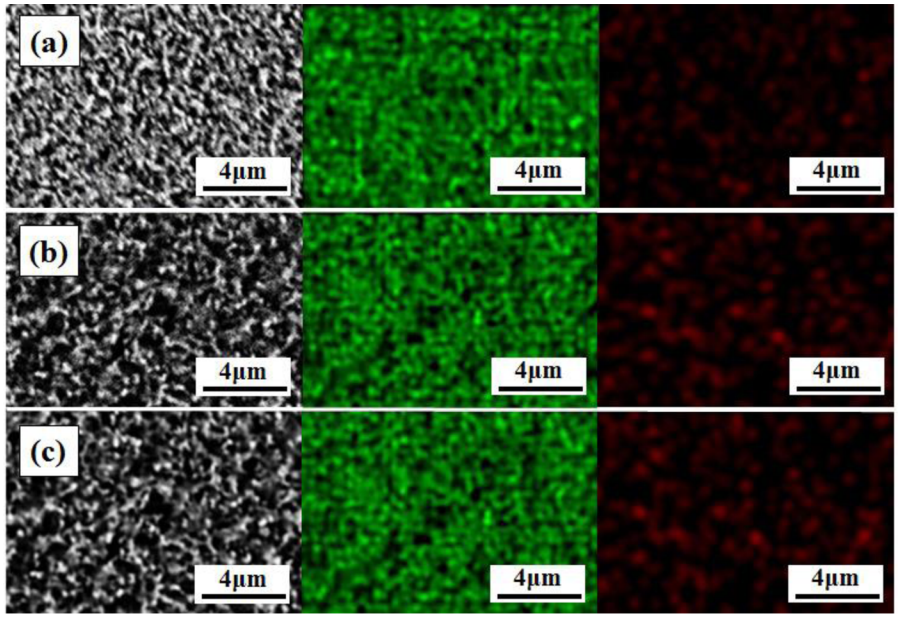

Figure 5. EDS elemental mapping of AuNPs-nSi top surface after (a) 5 s, (b) 10 s, and (c) 15 s 2nd electroless grafting processes. Left, original SEM image; middle, Si element (green); right image, Au element (red).

DOI: 10.1021/acsami.5b07395
ACS Appl. Mater. Interfaces 2015, 7, 22630−22637

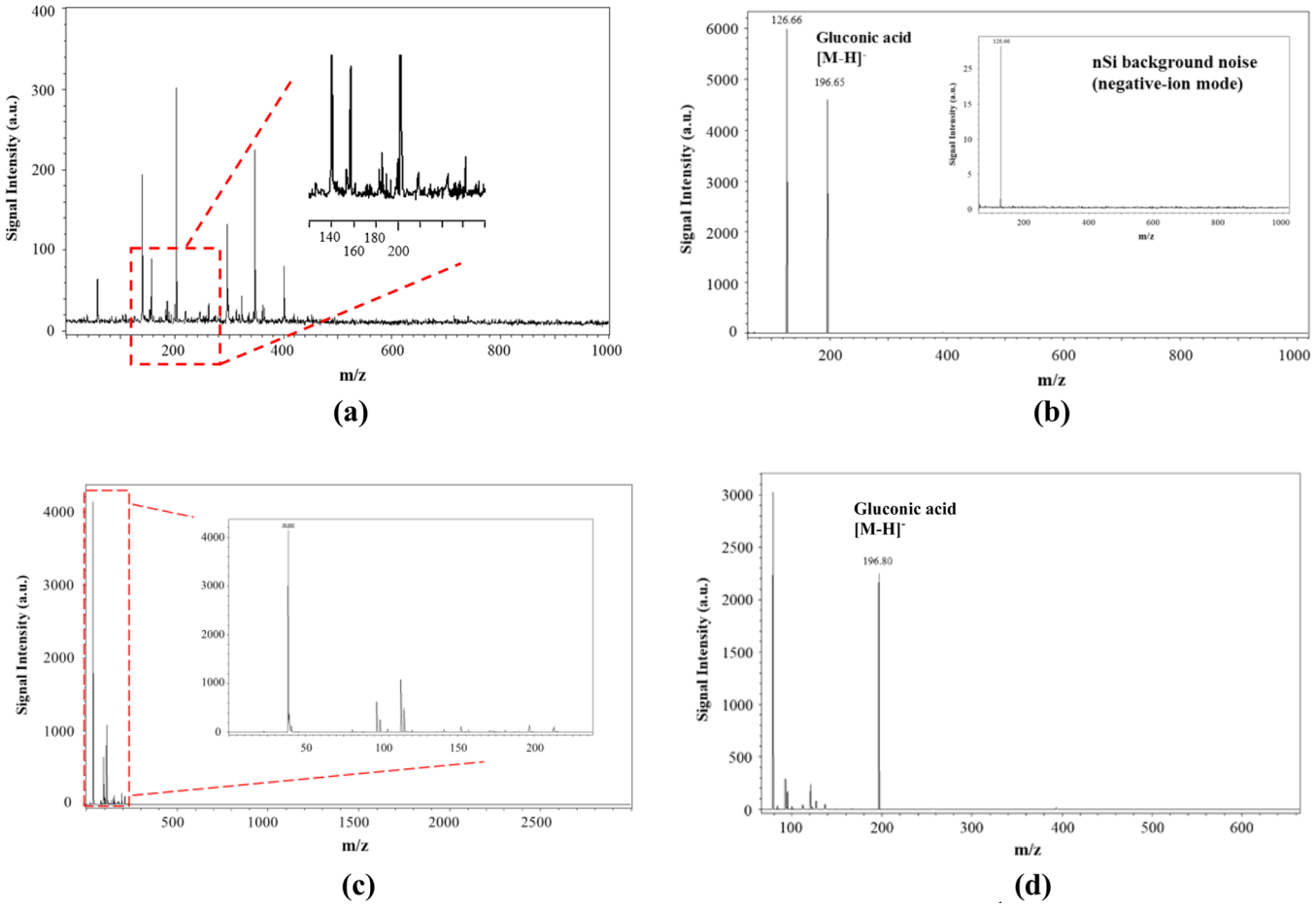

Figure 6. MS spectra of (a) native nSi surface used to detect a 10^{-1} M glucose sample in positive-ion mode and (b) AuNPs-nSi surface used to detect a 10^{-4} M glucose sample in negative-ion mode. The top-right corner shows the background noise of a AuNPs-nSi chip in negative-ion mode with no sample. Direct urine analysis of glucose on the AuNPs-nSi surface in (c) positive and (d) negative ion mode. The AuNPs-nSi surface was fabricated through deposition for 30 s and grafting for 15 s.

during sample preparation and chip fabrication procedures. Although glucose sample deposited on a nanostructure-based surface could be ionized by sodium and potassium ion adducts, the low sensitivity and specificity nSi-MS analysis results showed that native nSi is not an ideal approach for glucose detection. To overcome this limitation, we propose a novel method using Au-grafted nanoparticles to catalyze glucose into gluconic acid and directly perform nSi-MS analysis on a single AuNPs-nSi surface.

In AuNPs-nSi MS analysis, the sample was deposited on the AuNPs-nSi surface and allowed to react for 900 s for a sufficient catalysis reaction to occur.[48] The glucose samples on the AuNPs-nSi surface experienced two major stages for MS analysis. First, the desorption stage, in which the pulse laser energy emitted from the mass spectrometer was absorbed by the high surface-to-area ratio AuNPs-nSi surface, facilitating desorption of the glucose sample from the AuNPs-nSi surface by a thermal mechanism.[49] Second, the ionization stage, in which the glucose samples were catalyzed to negatively charged gluconic acid molecules by the on-chip AuNPs-nSi surface Au-based catalyst reactions. The ionized glucose samples were then effectively transported to a mass spectrometer analyzer for MS analysis. Figure 6b shows the MS spectra of a 10^{-4} M glucose sample deposited on the AuNPs-nSi surface. Because the gluconic acid was negatively charged after the Au catalyst reaction, the MS analysis was conducted in negative-ion mode. High MS detection sensitivity and specificity were achieved on the AuNPs-nSi surface, and two major peaks at 126 and 196 m/z were repeatedly observed in the MS spectra. The 196 m/z peak was identified as a gluconic acid sample ($[M - H]^-$, MW: 195) with a high detection sensitivity intensity of 4593 and a signal-to-noise (S/N) ratio of 1528. Compared with the AuNPs-nSi MS background noise spectra without a glucose sample, as shown in the top-right corner of Figure 6b. The 126 m/z signal peak was caused directly by the AuNPs-nSi surface instead of the glucose sample. The sharp unknown peak at 126 m/z may have been caused by the contaminates generated during wet etching or within the sample.

Glucose Analysis of a Urine Sample. The effectiveness of AuNPs-nSi in practical application was tested by analyzing glucose in a urine sample, which induces various noise interference and ion suppression problems for conventional MS analysis. Figure 6c shows direct AuNPs-nSi analysis of a urine sample operating in positive ion mode. Similar to the standard glucose sample analysis results, numerous MS peaks are oberved below 250 m/z. A sharp MS peak at 38.68 m/z indicates high potassium ions in the urine sample. No glucose molecule signal peaks were observed in the positive ion mode. Comparing the nSi-MS operated in positive mode, AuNPs-nSi in negative ion mode is a high-sensitivity and -spectificity MS analysis technique that can be used for urine analysis. Figure 6d shows the direct AuNPs-nSi MS analysis spectrum from the

DOI: 10.1021/acsami.5b07395
ACS Appl. Mater. Interfaces 2015, 7, 22630−22637

urine sample with a 5×10^{-4} M glucose concentration. One sharp peak at 196 m/z can clearly be identified in the AuNPs-nSi MS analysis results. Little background noise was found in the MS spectrum, showing the superior detection sensitivity and specificity for glucose in the urine sample of the AuNPs-nSi.

AuNPs-nSi MS Desorption/Ionization and Repeatability Tests. The glucose D/I efficiency and repeatability of AuNPs-nSi surfaces was evaluated by characterizing the gluconic acid ion signal intensity and S/N ratio. Figure 7 shows the MS signal intensity and S/N ratio after 5 s (Figure 7a), 10 s (Figure 7b), and 15 s (Figure 7c) Au grafting processes with series standard glucose sample concentrations ranging from 10^{-1} M to 10^{-8} M. The AuNPs-nSi MS repeatability was tested using three individual glucose MS measurements, and each MS spectrum is shown in the Supporting Information (Figures S2–S25). The average signal intensity, S/N value, and error bars are shown in Figure 7. In the tests, all AuNPs-nSi surfaces indicated the high detection sensitivity and high MS detection specificity of the method compared with current glucose detection methods. The detection signal intensity and S/N ratio were linearly correlated with the glucose sample concentration. For the AuNPs-nSi surface grafted for 5 s, the MS intensity ranged from 420 to 2130 and the S/N ratio ranged from 136 to 660 with a linear range from 10^{-1} to 10^{-8} M ($R^2 = 0.93$). When the grafting time was increased to 10 s, the MS detection sensitivity increased from 368 to 2661, and the S/N ratio ranged from 168 to 837 with a linear range from 10^{-1} to 10^{-8} M ($R^2 = 0.95$). For the AuNPs-nSi surface grafted for 15 s, an ultrahigh MS detection sensitivity of 10327 and S/N ratio of 3084 were observed for a 10^{-1} M glucose sample concentration. Even at the lowest sample concentration condition of 10^{-8} M, the AuNPs-nSi surface grafted for 15 s showed a high detection sensitivity of 1680 and S/N ratio of 499 with a linear range from 10^{-1} to 10^{-8} M ($R^2 = 0.93$). The detection limit of the 15 s AuNPs-nSi surface is 10^{-10} M.

The MS D/I efficiency results in Figure 7 indicate that, as the grafting time increases, a higher D/I efficiency is achieved. This is primarily because, as the grafting time increases, more Au nanoparticles graft to the nSi surface, resulting in more glucose molecules converting to gluconic acid molecules and, thus, enhancing the detection sensitivity. This observation is consistent with the EDS measurements summarized in Table 1.

Another potential reason for the efficiency increase is the AuNPs-nSi surface wettability. The AuNPs-nSi surface wettability varied with the grafting time. The SEM images presented in Figure 3 show that the AuNPs-nSi pore diameter increased with the grafting time with the same morphology. At the water contact angles shown in Figure 8, the contact angle decreased from 145° to 132°, 126°, and 93° for 5 s (Figure 8a), 10 s (Figure 8b), and 15 s (Figure 8c) grafting times, respectively. Larger pore sizes with lower surface wettability provide superior analyte penetration into the AuNPs-nSi surface and a stronger sample reaction. However, lower wettability with larger pore size may present side effects, reducing nSi D/I efficiency by lowering the local concentration.[9] We find that the 15 s Au grafting time was the optimal AuNPs-nSi condition for glucose sensing, providing more than 4-fold enhancement in D/I efficiency compared with the 5 s grafting condition.

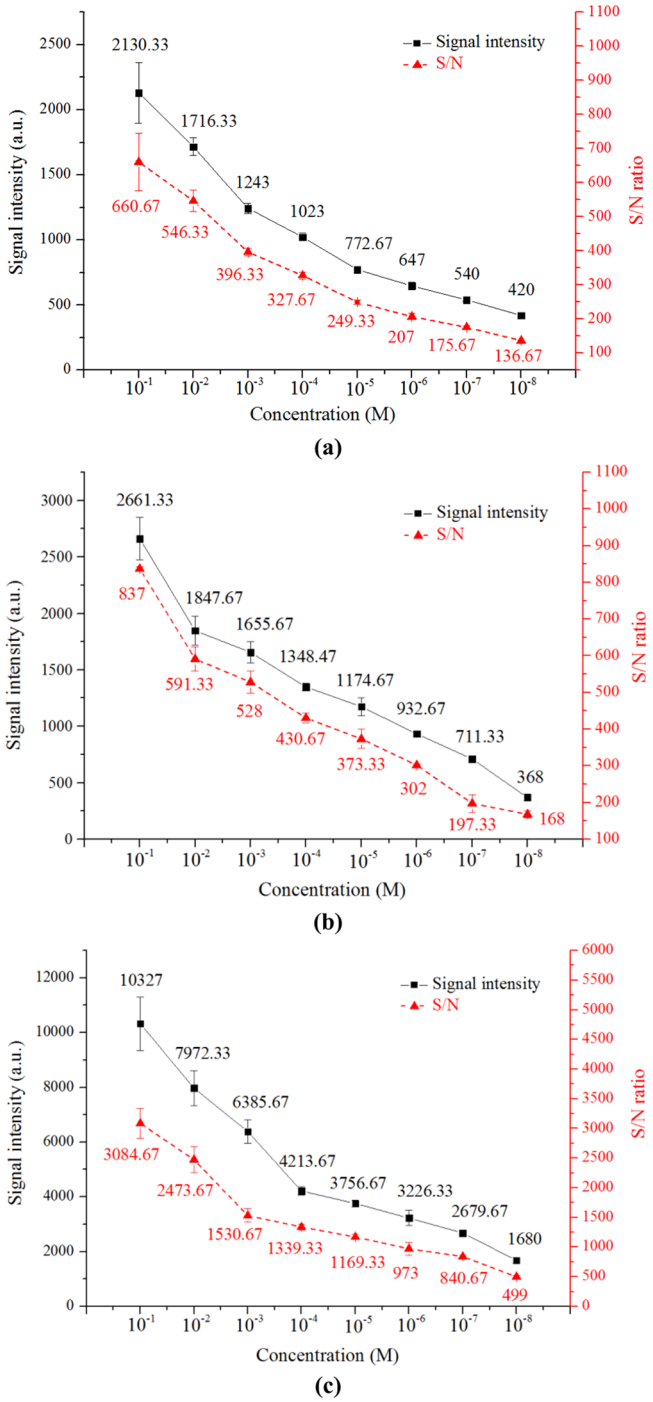

Figure 7. Glucose detection D/I efficiency in MS analysis of the AuNPs-nSi grafted for (a) 5 s, (b) 10 s, and (c) 15 s with glucose concentrations ranging from 10^{-1} to 10^{-8} M. The average signal intensity, S/N value, and error bars were obtained from three individual MS measurements.

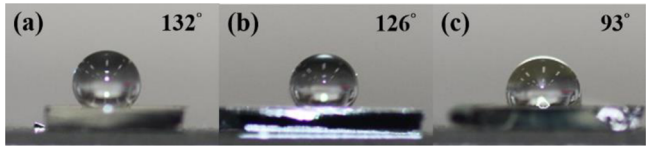

Figure 8. Water contact angle after (a) 5 s, (b) 10 s, and (c) 15 s 2nd Au grafting to the AuNPs-nSi surface.

DOI: 10.1021/acsami.5b07395
ACS Appl. Mater. Interfaces 2015, 7, 22630–22637

CONCLUSIONS

A novel approach to analyzing AuNPs-nSi surfaces was successfully demonstrated using a matrix-free DIOS-MS approach with high sensitivity and detection specificity for glucose analysis. The AuNPs-nSi was fabricated using Au deposition, grafting, and metal-assisted etching steps. The entire AuNPs-nSi fabrication procedure was a full-wet process and required no high-cost equipment to generate a nanostructure-based silicon surface. Glucose samples on the AuNPs-nSi surface were directly catalyzed to negatively charged gluconic acid molecules using Au nanoparticles and desorbed from the AuNPs-nSi surface for MS analysis.

The effects of the deposition and grafting parameters on the glucose D/I efficiency were analyzed. The results showed that the AuNPs-nSi surface subjected to deposition for 30 s and grafting for 15 s exhibited optimal D/I efficiency for glucose catalysis reaction and nSi-MS desorption/ionization. A high MS signal intensity of 1680 and an S/N ratio of 499 were achieved at a low glucose level of 10^{-8} M. Furthermore, glucose in the urine sample was detected to demonstrate the effectiveness of the AuNPs-nSi MS technique in practical applications. This study showed that AuNPs-nSi MS analysis has high detecion sensitivity and specificity for determining the glucose level in a biological sample compared with current glucose-sensing techniques. This technique shows great potential for further applications, such as identification of glucose molecules in real samples[45] or MS imaging.[21]

ASSOCIATED CONTENT

Supporting Information

The Supporting Information is available free of charge on the ACS Publications website at DOI: 10.1021/acsami.5b07395.

FESEM images and individual MS spectra of glucose sampling (PDF)

AUTHOR INFORMATION

Corresponding Author

*E-mail: cwtsao@ncu.edu.tw.

Notes

The authors declare no competing financial interest.

ACKNOWLEDGMENTS

The authors thank the Ministry of Science and Technology, Taiwan, for financially supporting this project (MOST 103-2221-E-008-027), Dr. Yu-Liang Yang in Agricultural Biotechnology Research Center, Academia Sinica, Taiwan for providing the MS spectrometer, and NCU precious instruments utilization center for providing FESEM and EDS instruments.

REFERENCES

(1) Fenn, J.; Mann, M.; Meng, C.; Wong, S.; Whitehouse, C. Electrospray ionization for mass spectrometry of large biomolecules. *Science* **1989**, *246* (4926), 64−71.

(2) Tanaka, K.; Waki, H.; Ido, Y.; Akita, S.; Yoshida, Y.; Yoshida, T.; Matsuo, T. Protein and polymer analyses up to m/z 100 000 by laser ionization time-of-flight mass spectrometry. *Rapid Commun. Mass Spectrom.* **1988**, *2* (8), 151−153.

(3) Karas, M.; Hillenkamp, F. Laser desorption ionization of proteins with molecular masses exceeding 10,000 Da. *Anal. Chem.* **1988**, *60* (20), 2299−2301.

(4) Wei, J.; Buriak, J. M.; Siuzdak, G. Desorption-ionization mass spectrometry on porous silicon. *Nature* **1999**, *399* (6733), 243−246.

(5) Northen, T. R.; Yanes, O.; Northen, M. T.; Marrinucci, D.; Uritboonthai, W.; Apon, J.; Golledge, S. L.; Nordstrom, A.; Siuzdak, G. Clathrate nanostructures for mass spectrometry. *Nature* **2007**, *449* (7165), 1033−U3.

(6) Go, E. P.; Apon, J. V.; Luo, G.; Saghatelian, A.; Daniels, R. H.; Sahi, V.; Dubrow, R.; Cravatt, B. F.; Vertes, A.; Siuzdak, G. Desorption/Ionization on Silicon Nanowires. *Anal. Chem.* **2005**, *77* (6), 1641−1646.

(7) Tsao, C. W.; Kumar, P.; Liu, J. K.; Devoe, L. Dynamic electrowetting on nanofilament silicon for matrix-free laser desorption/ionization mass spectrometry. *Anal. Chem.* **2008**, *80* (8), 2973−2981.

(8) Tsao, C. W.; Lin, C. H.; Cheng, Y. C.; Chien, C. C.; Chang, C. C.; Chen, W. Y. Nanostructured silicon surface modifications for as a selective matrix-free laser desorption/ionization mass spectrometry. *Analyst* **2012**, *137* (11), 2643−50.

(9) Chen, W. Y.; Huang, J. T.; Cheng, Y. C.; Chien, C. C.; Tsao, C. W. Fabrication of nanostructured silicon by metal-assisted etching and its effects on matrix-free laser desorption/ionization mass spectrometry. *Anal. Chim. Acta* **2011**, *687* (2), 97−104.

(10) Wang, Y. D.; Zeng, Z. F.; Li, J.; Chi, L. F.; Guo, X. H.; Lu, N. Biomimetic Antireflective Silicon Nanocones Array for Small Molecules Analysis. *J. Am. Soc. Mass Spectrom.* **2013**, *24* (1), 66−73.

(11) Wang, Y. B.; Chen, W.; Wu, J. S.; Guo, Y. L.; Xia, X. H. Highly efficient and of selective enrichment phosphopeptides using porous anodic alumina membrane for MALDI-TOF MS analysis. *J. Am. Soc. Mass Spectrom.* **2007**, *18* (8), 1387−1395.

(12) Gulbakan, B.; Park, D.; Kang, M. C.; Kececi, K.; Martin, C. R.; Powell, D. H.; Tan, W. H. Laser Desorption Ionization Mass Spectrometry on Silicon Nanowell Arrays. *Anal. Chem.* **2010**, *82* (18), 7566−7575.

(13) Trauger, S. A.; Go, E. P.; Shen, Z.; Apon, J. V.; Compton, B. J.; Bouvier, E. S. P.; Finn, M. G.; Siuzdak, G. High Sensitivity and Analyte Capture with Desorption/Ionization Mass Spectrometry on Silylated Porous Silicon. *Anal. Chem.* **2004**, *76* (15), 4484−4489.

(14) Shen, Z. X.; Thomas, J. J.; Siuzdak, G.; Blackledge, R. D. A case study on forensic polymer analysis by DIOS-MS: The suspect who gave us the SLIP (R). *J. Forensic Sci.* **2004**, *49* (5), 1028−1035.

(15) Cheng, Y. C.; Chen, K. H.; Wang, J. S.; Hsu, W. L.; Chien, C. C.; Chen, W. Y.; Tsao, C. W. Rapid analysis of abused drugs using nanostructured silicon surface assisted laser desorption/ionization mass spectrometry. *Analyst* **2012**, *137* (3), 654−61.

(16) Guinan, T.; Ronci, M.; Kobus, H.; Voelcker, N. H. Rapid detection of illicit drugs in neat saliva using desorption/ionization on porous silicon. *Talanta* **2012**, *99*, 791−798.

(17) Dupre, M.; Coffinier, Y.; Boukherroub, R.; Cantel, S.; Martinez, J.; Enjalbal, C. Laser desorption ionization mass spectrometry of protein tryptic digests on nanostructured silicon plates. *J. Proteomics* **2012**, *75* (7), 1973−1990.

(18) Yanes, O.; Woo, H. K.; Northen, T. R.; Oppenheimer, S. R.; Shriver, L.; Apon, J.; Estrada, M. N.; Potchoiba, M. J.; Steenwyk, R.; Manchester, M.; Siuzdak, G. Nanostructure Initiator Mass Spectrometry: Tissue Imaging and Direct Biofluid Analysis. *Anal. Chem.* **2009**, *81* (8), 2969−2975.

(19) Liu, Q.; Guo, Z.; He, L. Mass spectrometry imaging of small molecules using desorption/ionization on silicon. *Anal. Chem.* **2007**, *79* (10), 3535−3541.

(20) Goodwin, R. J. A.; Pennington, S. R.; Pitt, A. R. Protein and peptides in pictures: Imaging with MALDI mass spectrometry. *Proteomics* **2008**, *8* (18), 3785−3800.

(21) Chen, S. M.; Xiong, C. Q.; Liu, H. H.; Wan, Q. Q.; Hou, J.; He, Q.; Badu-Tawiah, A.; Nie, Z. X. Mass spectrometry imaging reveals the sub-organ distribution of carbon nanomaterials. *Nat. Nanotechnol.* **2015**, *10* (2), 176−182.

(22) Reach, G.; Wilson, G. S. Can Continuous Glucose Monitoring Be Used for the Treatment of Diabetes. *Anal. Chem.* **1992**, *64* (6), A381−A386.

DOI: 10.1021/acsami.5b07395
ACS Appl. Mater. Interfaces 2015, 7, 22630−22637

(23) Urakami, T.; Morimoto, S.; Nitadori, Y.; Harada, K.; Owada, M.; Kitagawa, T. Urine glucose screening program at schools in Japan to detect children with diabetes and its outcome-incidence and clinical characteristics of childhood type 2 diabetes in Japan. *Pediatr. Res.* **2007**, *61* (2), 141−145.
(24) Pickup, J. C.; Hussain, F.; Evans, N. D.; Rolinski, O. J.; Birch, D. J. S. Fluorescence-based glucose sensors. *Biosens. Bioelectron.* **2005**, *20* (12), 2555−2565.
(25) Steiner, M. S.; Duerkop, A.; Wolfbeis, O. S. Optical methods for sensing glucose. *Chem. Soc. Rev.* **2011**, *40* (9), 4805−4839.
(26) Weiss, R.; Yegorchikov, Y.; Shusterman, A.; Raz, I. Noninvasive continuous glucose monitoring using photoacoustic technology - Results from the first 62 subjects. *Diabetes Technol. Ther.* **2007**, *9* (1), 68−74.
(27) Su, L.; Feng, J.; Zhou, X. M.; Ren, C. L.; Li, H. H.; Chen, X. G. Colorimetric Detection of Urine Glucose Based ZnFe2O4Magnetic Nanoparticles. *Anal. Chem.* **2012**, *84* (13), 5753−5758.
(28) Lu, C.; Liu, X. J.; Li, Y. F.; Yu, F.; Tang, L. H.; Hu, Y. J.; Yine, Y. B. Multifunctional Janus Hematite Silica Nanoparticles: Mimicking Peroxidase-Like Activity and Sensitive Colorimetric Detection of Glucose. *ACS Appl. Mater. Interfaces* **2015**, *7* (28), 15395−15402.
(29) Hsieh, H. V.; Pfeiffer, Z. A.; Amiss, T. J.; Sherman, D. B.; Pitner, J. B. Direct detection of glucose by surface plasmon resonance with bacterial glucose/galactose-binding protein. *Biosens. Bioelectron.* **2004**, *19* (7), 653−660.
(30) Chen, C.; Xie, Q. J.; Yang, D. W.; Xiao, H. L.; Fu, Y. C.; Tan, Y. M.; Yao, S. Z. Recent advances in electrochemical glucose biosensors: a review. *RSC Adv.* **2013**, *3* (14), 4473−4491.
(31) Wang, J. Electrochemical glucose biosensors. *Chem. Rev.* **2008**, *108* (2), 814−825.
(32) Harper, A.; Anderson, M. R. Electrochemical Glucose Sensors-Developments Using Electrostatic Assembly and Carbon Nanotubes for Biosensor Construction. *Sensors* **2010**, *10* (9), 8248−8274.
(33) Tian, K.; Prestgard, M.; Tiwari, A. A review of recent advances in nonenzymatic glucose sensors. *Mater. Sci. Eng., C* **2014**, *41*, 100−118.
(34) Park, S.; Boo, H.; Chung, T. D. Electrochemical non-enzymatic glucose sensors. *Anal. Chim. Acta* **2006**, *556* (1), 46−57.
(35) Toghill, K. E.; Compton, R. G. Electrochemical Non-enzymatic Glucose Sensors: A Perspective and an Evaluation. *Int. J. Electrochem. Sci.* **2010**, *5* (9), 1246−1301.
(36) Oliver, N. S.; Toumazou, C.; Cass, A. E. G.; Johnston, D. G. Glucose sensors: a review of current and emerging technology. *Diabetic Med.* **2009**, *26* (3), 197−210.
(37) Vaddiraju, S.; Burgess, D. J.; Tomazos, I.; Jain, F. C.; Papadimitrakopoulos, F. Technologies for Continuous Glucose Monitoring: Current Problems and Future Promises. *J. Diabetes Sci. Technol.* **2010**, *4* (6), 1540−1562.
(38) Birsoy, K.; Possemato, R.; Lorbeer, F. K.; Bayraktar, E. C.; Thiru, P.; Yucel, B.; Wang, T.; Chen, W. W.; Clish, C. B.; Sabatini, D. M. Metabolic determinants of cancer cell sensitivity to glucose limitation and biguanides. *Nature* **2014**, *508* (7494), 108−112.
(39) Hirayama, A.; Kami, K.; Sugimoto, M.; Sugawara, M.; Toki, N.; Onozuka, H.; Kinoshita, T.; Saito, N.; Ochiai, A.; Tomita, M.; Esumi, H.; Soga, T. Quantitative Metabolome Profiling of Colon and Stomach Cancer Microenvironment by Capillary Electrophoresis Time-of-Flight Mass Spectrometry. *Cancer Res.* **2009**, *69* (11), 4918−4925.
(40) Taormina, C. R.; Baca, J. T.; Asher, S. A.; Grabowski, J. J.; Finegold, D. N. Analysis of tear glucose concentration with electrospray ionization mass spectrometry. *J. Am. Soc. Mass Spectrom.* **2007**, *18* (2), 332−336.
(41) McIntosh, T. S.; Davis, H. M.; Matthews, D. E. A liquid chromatography-mass spectrometry method to measure stable isotopic tracer enrichments of glycerol and glucose in human serum. *Anal. Biochem.* **2002**, *300* (2), 163−169.
(42) Bruggink, C.; Maurer, R.; Herrmann, H.; Cavalli, S.; Hoefler, F. Analysis of carbohydrates by anion exchange chromatography and mass spectrometry. *J. Chromatogr A* **2005**, *1085* (1), 104−109.
(43) He, Q.; Chen, S.; Wang, J.; Hou, J.; Xiong, S.; Nie, Z. 1-naphthylhydrazine hydrochloride: a new matrix for the quantification of glucose and homogentisic acid in real samples by MALDI-TOF MS. *Clin. Chim. Acta* **2013**, *420*, 94−8.
(44) Chen, R.; Xu, W.; Xiong, C.; Zhou, X.; Xiong, S.; Nie, Z.; Mao, L.; Chen, Y.; Chang, H.-C. High-Salt-Tolerance Matrix for Facile Detection of Glucose in Rat Brain Microdialysates by MALDI Mass Spectrometry. *Anal. Chem.* **2012**, *84* (1), 465−469.
(45) Chen, S. M.; Zheng, H. Z.; Wang, J. N.; Hou, J.; He, Q.; Liu, H. H.; Xiong, C. Q.; Kong, X. L.; Nie, Z. X. Carbon Nanodots As a Matrix for the Analysis of Low-Molecular-Weight Molecules in Both Positive- and Negative-Ion Matrix-Assisted Laser Desorption/Ionization Time-of-Flight Mass Spectrometry and Quantification of Glucose and Uric Acid in Real Samples. *Anal. Chem.* **2013**, *85* (14), 6646−6652.
(46) Li, X.; Bohn, P. W. Metal-assisted chemical etching in HF/H[sub 2]O[sub 2] produces porous silicon. *Appl. Phys. Lett.* **2000**, *77* (16), 2572.
(47) Huang, Z. P.; Geyer, N.; Werner, P.; de Boor, J.; Gosele, U. Metal-Assisted Chemical Etching of Silicon: A Review. *Adv. Mater.* **2011**, *23* (2), 285−308.
(48) Comotti, M.; Della Pina, C.; Matarrese, R.; Rossi, M. The catalytic activity of "naked" gold particles. *Angew. Chem., Int. Ed.* **2004**, *43* (43), 5812−5.
(49) Li, J.; Lipson, R. H. Insights into Desorption Ionization on Silicon (DIOS). *J. Phys. Chem. C* **2013**, *117* (51), 27114−27119.

DOI: 10.1021/acsami.5b07395
ACS Appl. Mater. Interfaces 2015, 7, 22630−22637